PHYSICAL REVIEW B VOLUME 31, NUMBER 8 15 APRIL 1985

Vibrational relaxation and electronic energy transfer of N_2 aggregates in solid Xe matrices

H. Kühle, J. Bahrdt, R. Fröhling, and N. Schwentner
Institut für Atom- und Festkörperphysik, Freie Universität Berlin, Arnimallee 14, 1000 Berlin 33, Federal Republic of Germany

H. Wilcke
Institut für Experimentalphysik, Universität Kiel, Olshausenstrasse 40-60, 2300 Kiel, Federal Republic of Germany

(Received 3 December 1984)

Population distributions of vibrational levels within the first excited electronic state $A\ ^3\Sigma_u^+$ of N_2 molecules embedded in a Xe matrix have been derived from emission spectra resulting from selective excitation of individual levels with monochromatized synchrotron radiation. The steady-state population distributions strongly depend on the originally excited level and are incompatible with a simple stepwise nonradiative relaxation process between successive vibrational levels. The experimental distributions are attributed to relaxation by nonradiative electronic energy transfer processes between neighboring N_2 molecules via exchange interaction. The cascade in the $A\ ^3\Sigma_u^+$ state involves relaxation to lower energies in steps of two vibrational quanta and an up conversion of the energy in steps of three vibrational quanta. The probability of these processes follows an energy-gap law for the excess energy.

I. INTRODUCTION

Rate constants for vibrational relaxation in the solid state cover a range of about ten orders of magnitude.[1,2] N_2 molecules in N_2 crystals and isolated in rare-gas matrices represent a well-known case of very slow vibrational relaxation. The interaction of long-living vibrational levels in the electronic ground state of N_2 crystals with electronically excited N atoms has been studied in detail[3] with interesting results concerning relaxation and energy transfer. The lowest electronically excited state $A\ ^3\Sigma_u^+$ of N_2 molecules in rare-gas matrices is the best example for slow vibrational relaxation of an excited electronic state in the solid phase with rate constants below 1 s^{-1} for completely isolated molecules.[4] Such a slow vibrational relaxation has been predicted theoretically[5] and verified experimentally[4–11] more than a decade ago. Also relaxation within higher electronic states[7,10–13] has been investigated. The $A\ ^3\Sigma_u$ state excited in small N_2 aggregates which are distributed in a rare-gas matrix might be suitable for a case study of the conversion of different vibrational and electronic degrees of freedom of a cluster into matrix phonons. This system has the advantage that only two electronic states, the $A\ ^3\Sigma_u^+$ state and the $X\ ^1\Sigma_g^+$ ground state are involved if we restrict ourselves to $v' \leq 6$. Furthermore, the vibrational quanta of the N_2 excited state, the N_2 ground state, and the rare-gas matrix have energies of about 174, 292, and 5 meV, respectively, and are easily distinguishable in the experiments. In earlier studies[3,4,6–10,13] the samples have been excited by x-rays or electrons which populate many electronic and vibrational states by energy loss processes. The observation of emission from $v'=0$ up to $v'=6$ of $A\ ^3\Sigma_u^+$ in luminescence spectra and the absence of a rise time, both for low N_2 concentrations, shows that cascading of single N_2 molecules in rare gas matrices during the radiative decay time can be neglected. On the other hand it is known that pure solid N_2 emits only from the two lowest vibrational levels of $A\ ^3\Sigma_u^+$.[14] Therefore the relaxation processes can be controlled experimentally by increasing the N_2 concentration in the matrix and relaxation processes for example of two N_2 molecules separated by one matrix atom or of N_2 pairs or of larger clusters can be studied.

For an investigation of vibrational relaxation in N_2 clusters it is desirable to populate selectively a specific vibrational level in the $A\ ^3\Sigma_u^+$ state and to monitor all intermediate steps in the subsequent relaxation cascade. In this paper, population distributions due to vibrational relaxation in N_2 clusters are reported which have been derived from luminescence spectra after selective excitation of individual vibrational levels by light.[11] Optical transitions between the $A\ ^3\Sigma_u^+$ state and the $X\ ^1\Sigma_g^+$ ground state are forbidden according to spin-selection rules. These selection rules were weakened in matrices of high atomic weight.[4] Xe has been used as matrix because it induces the strongest $A\ ^3\Sigma_u^+ \leftrightarrow X\ ^1\Sigma_g^+$ optical transition probability corresponding to a lifetime of $1.5 \pm 0.5 \times 10^{-3}$ s.[15] Thus the absorption coefficient is sufficient for excitation of about 1-mm thick films doped with 0.1% N_2 molecules. Furthermore, the faster radiative decay rate allows for an effective competition with vibrational relaxation and the emission spectra also reflect the intermediate steps in the relaxation cascade and not only the final state of accumulation in the lowest levels. The population distributions presented here show that vibrational relaxation in N_2 aggregates does not follow the simple way from one vibrational level to the next lower vibrational level by dissipation of the excess energy into phonons. The relaxation

proceeds via an interplay of nonresonant electronic energy transfer processes involving conversion of vibrational energy of the excited electronic state into vibrational energy of the electronic ground state. The guide line in the selection of the efficient pathways out of the large number of possible nonresonant transfer processes is the minimalization of the excess energy which has to be converted into phonons. In the course of relaxation vibrational energy is also transferred back from the electronic ground state into the excited state yielding an increase of the total energy accumulated in one N_2 molecule in this step. The experimental population distributions can be quantitatively modeled by a series of down and up conversion processes. The interpretation combines features of vibrational up conversion observed for example in the electronic ground state of CO and CN molecules in rare gas matrices[16] and of vibrational relaxation via a different intermediate electronic state observed for example for CN (Ref. 17) and $(O_2)_2$ (Ref. 18) in rare-gas matrices.

The dissipation of the excess energy into phonons is governed by the coupling of the involved electronic transitions to the lattice. The coupling strength is reflected in the line shape of the optical transition. The line shapes of transitions to singlet states of N_2 molecules have been analyzed in a convincing way in terms of electron-phonon coupling.[19] Here we present absorption and emission spectra of triplet transitions ($\Delta S=1$) of the N_2 molecule in a Xe matrix. The transition energies yield immediately the excess energies involved in the relaxation processes and from the line shape the electron-phonon coupling strength is derived. Thus the rate constants for the up and down conversion processes contributing to the vibrational relaxation can be calculated without free parameters.

II. EXPERIMENTAL RESULTS

The experiments have been performed at the beam line SUPERLUMI at the storage ring DORIS in Hamburg. The set up provides a flux of about 10^{12} photons $nm^{-1}\,s^{-1}$ for excitation purposes with an ultimate resolution of 0.007 nm.[20] The luminescence light of the sample is analyzed by a $f/3$ monochromator at a resolution of 0.7 nm.[21] Xe and N_2 of 99.997% and 99.9992%, respectively, purity have been mixed in the gas phase with partial pressures corresponding to the concentration of the sample. The mixtures have been deposited as films on a LiF substrate cooled to 7 ± 2 K by a He flow cryostat with thicknesses of about 1 mm.

The transparent region of about 8 eV of a Xe matrix allows only absorption due to transitions from the lowest vibrational level of the $X\ ^1\Sigma_g^+$ ground state to the three lowest excited electronic states which are the $A\ ^3\Sigma_u^+$, $B\ ^3\Pi_g$, and $W\ ^3\Delta_u$ triplet states. We have observed vibrational progressions of the $A\ ^3\Sigma_u^+ \leftarrow X\ ^1\Sigma_g^+$ and $B\ ^3\Pi_g \leftarrow X\ ^1\Sigma_g^+$ transitions in absorption. The absorption cross sections are weak due to the spin-selection rule and the spectra show a strong background of luminescence and scattered light. Much nicer spectra are obtained in recording the total luminescence intensity versus the excitation wavelength which reflects the amount of absorbed light. The energy positions of the bands and the line shapes in these excitation spectra and in conventional absorption spectra are identical. The intensity of the bands could differ because of a wavelength dependence of the quantum efficiency of the sample and of the detection system. A comparison of excitation and absorption spectra shows that these differences are marginal. The $A\ ^3\Sigma_u^+$ vibrational progression for $v'=1$ to 12 and the $B\ ^3\Pi_g$ progression for $v'=0$ to 4 are displayed in the excitation spectrum of Fig. 1 for a sample of 2% N_2 in Xe. Beyond 150 nm the N_2 bands disappear in the absorption background of the matrix. The transition energies are listed in Table I together with the gas phase values. The line shapes of several $A\ ^3\Sigma_u$ vibrational bands taken with a resolution of 0.05 nm ($\approx$0.003 eV) are collected in Fig. 2.

In the following we will focus our attention on the $v'=1$ to 6 vibrational bands of the $A\ ^3\Sigma_u^+$ state. Each of these levels has been excited selectively. Typical luminescence spectra are shown in Fig. 3 for 2% N_2 in Xe. The spectra contain combinations of Vegard-Kaplan bands $A\ ^3\Sigma_u^+(v') \rightarrow X\ ^1\Sigma_g^+(v'')$ with different initial states v' and with vibrational progressions due to decay to several final vibrational states v''. Figure 3 demonstrates that only some of the vibrational levels v' below the initially excited level act as emitting states. There is a selective population of v' levels by vibrational relaxation. Furthermore, the distribution within the v' levels depends strongly on the choice of the initially excited level and on N_2 concentration (Fig. 3). The intensity of the emission bands allows for a quantitative determination of the population distribution within the $A\ ^3\Sigma_u^+(v')$ levels. The scheme of Fig. 4 illustrates that we are interested in the population N_i of the ith vibrational level of $A\ ^3\Sigma_u^+$. This level is populated from higher levels with intensities I_{ki} and rate constants w_{ki}. It is depopulated by nonradiative vibrational relaxation to lower levels with intensities and rate constants I_{ij} and w_{ij}. In addition we have radiative transitions to the ground state with intensities (number of photons) and rate constants I_{il} and w_{il}. The rate constants and the relative intensities and populations are connected for radiative decay and for the type of radiationless relaxation discussed here via

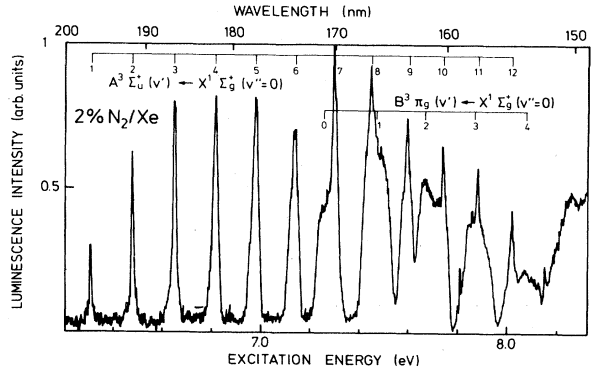

FIG. 1. Total luminescence intensity versus exciting photon energy showing the $A\ ^3\Sigma_u^+(v')$ and $B\ ^3\Pi_g^+(v')$ progressions for 2% N_2 in Xe at 7 K. This luminescence yield is similar to an absorption spectrum. The intensity is corrected for the incoming photon flux.

TABLE I. Energies of the maxima in the $A\ ^3\Sigma_u^+(v')\leftarrow X\ ^1\Sigma_g^+(v''=0)$ and the $B\ ^3\Pi_g(v')\leftarrow X\ ^1\Sigma_g^+(v''=0)$ transitions in absorption for 2% N_2/Xe at 7 K (energies in eV). The Stokes shift of the $A\ ^3\Sigma_u^+$ transition compared to the emission data of Tinti and Robinson (Ref. 4) corresponds to 7±1 meV for the listed values. The gas-phase energies (Ref. 23) are given for comparison.

	v'													
	0	1	2	3	4	5	6	7	8	9	10	11	12	13
Matrix														
$A\ ^3\Sigma_u^+$		6.307	6.486	6.652	6.819	6.982	7.142	7.298	7.454	7.602	7.748	7.886	8.022	8.159
$B\ ^3\Pi_g$	7.239	7.467	7.669	7.870	8.069									
Gas														
$A\ ^3\Sigma_u^+$	6.168	6.345	6.522	6.691	6.858	7.025	7.183	7.341	7.492	7.644	7.788	7.933	8.072	8.201
$B\ ^3\Pi_g$	7.354	7.565	7.773	7.979	8.178									

$$I_{nm}=w_{nm}N_n\ . \tag{1}$$

The experiments are carried out under steady-state conditions (repetition rate of excitation 5×10^8 Hz, decay rate 10^3 Hz) and all quantities are independent on time. The radiative rate constants follow from[22]

$$w_{il}=\nu_{il}^3\mathcal{F}(i,l)R_e^2\ , \tag{2}$$

with the transition frequency ν_{il}, the Franck-Condon factor $\mathcal{F}(i,l)$, and the dipole matrix element R_e^2 which does not depend on i and l in the Franck-Condon approximation. The intensity I_{il} of any band in a progression starting from v' can be used to derive the population N_i of this level v' relative to the population of all other vibrational levels in the cascade by[22]

$$N_i=I_{il}\Big/\left[\nu_{il}^3\mathcal{F}(i,l)\sum_{l'}\left|I_{il'}/\nu_{il'}^3\mathcal{F}(i,l')\right|\right]\ . \tag{3}$$

In the evaluation we used a mean value obtained from several strong bands in a progression. The derived population distributions are listed in Table II and displayed as histograms in Fig. 5. The length of the bars in a vertical histogram represents the population. The arrows mark the initially populated levels and the parabola to the left illustrates the $A\ ^3\Sigma_u^+$ state with its vibrational levels.

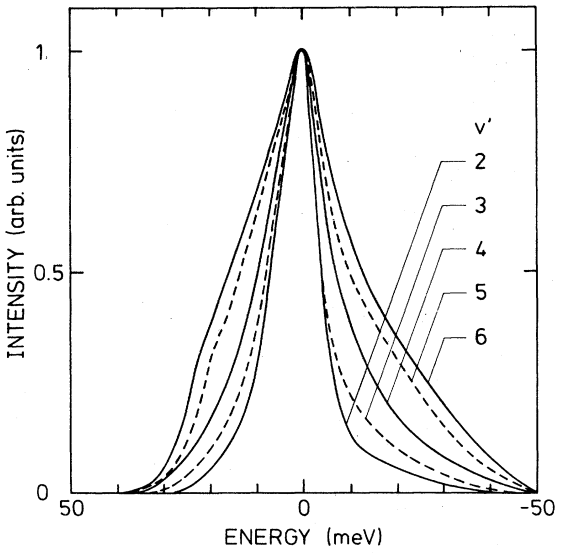

FIG. 2. Line shape of the $A\ ^3\Sigma_u^+(v')\leftarrow X\ ^1\Sigma_g^+(v''=0)$ absorption bands for $2\le v'\le 6$.

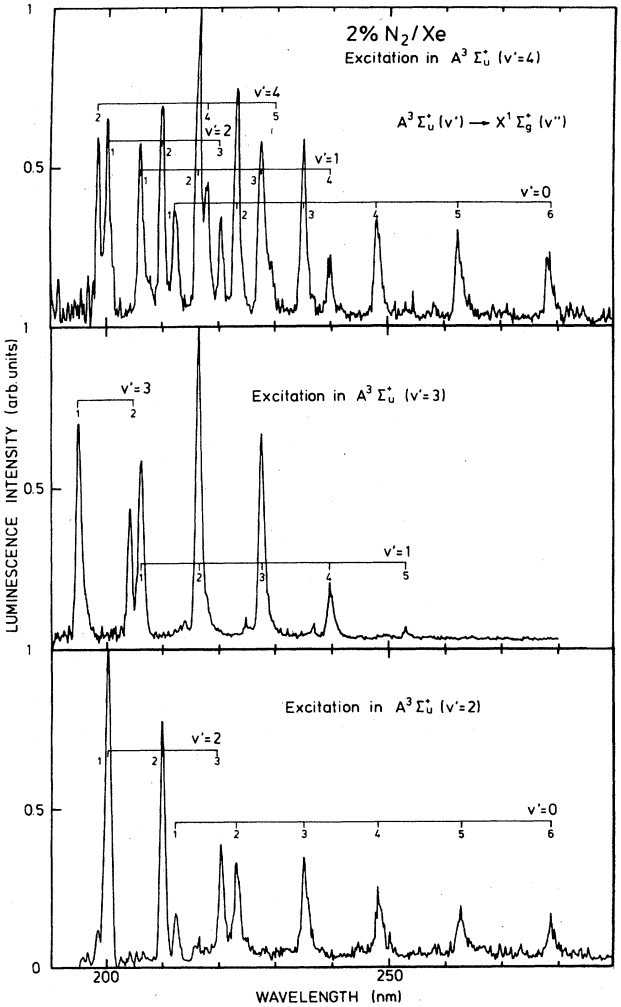

FIG. 3. Luminescence emission spectra with $A\ ^3\Sigma_u^+(v')\rightarrow X\ ^1\Sigma_g^+(v'')$ Vegard-Kaplan bands for excitation of $v'=2$, 3, and 4 of $A\ ^3\Sigma_u^+$, 2% N_2 in Xe at 7 K. The spectra are not corrected for the detection efficiency.

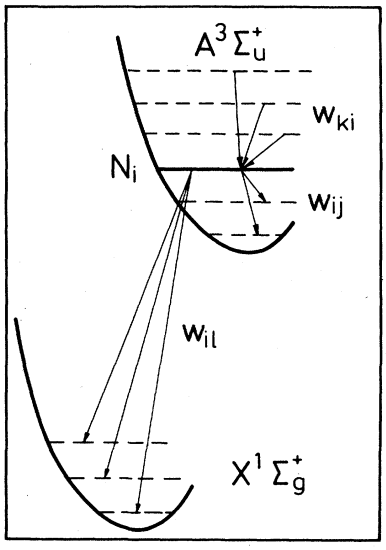

FIG. 4. Scheme for population of a level i by nonradiative rate constants w_{ki} and for depopulation of level i by radiative rate constants w_{il} and nonradiative rate constants w_{ij}.

The information used so far is sufficient to give these relative population distributions in a unique way. But the question whether the populations in one histogram add up to 100% of the deposited number of photons /s or whether there are some hidden populations of other states is open. To answer this question we need the quantum efficiency (ratio of deposited to emitted photons) of the sample. Excitation spectra and absorption spectra are connected via the quantum efficiency. The intensity distribution of the $A\ ^3\Sigma_u^+(1 \leq v' \leq 6)$ levels is very similar in excitation and absorption spectra and it follows the known Franck-Condon factors.

Evidently the quantum efficiency is the same for all these vibrational levels. Some further experimental information indicates that q is even near unity. An estimate using the measured absolute photon flux of the excitation set up at the sample and the efficiency of the detection system for luminescence yields $q \approx 1$ with an uncertain order of magnitude. Transmission measurements of thick films yield a more accurate value. The expected minima in transmission spectra due to absorption bands are converted to maxima for large film thicknesses. The detector receives transmitted light and a background from luminescence and elastically scattered light. In the center of an absorption band the amount of transmitted light is very low. Most of the light is absorbed and converted to luminescence light. The signal is dominated by luminescence. Outside the band only few photons are absorbed and the luminescence contribution is negligible. But also the transmitted part is small for thick samples because most of the light is scattered. The intensity ratio inside the band (I_{lum}) and outside the band (I_{scat}) is given by

$$I_{\text{lum}}/I_{\text{scat}} = q\eta_{\text{lum}}/\eta_{\text{scat}}\ , \tag{4}$$

for an isotropic distribution of luminescence and scattered light provided that the sample is sufficiently thick to prevent transmission. The detection efficiency η_{lum} for the longer-wavelength luminescence is higher than η_{scat} for the shorter wavelength of elastically scattered light. For a sufficiently high quantum efficiency q, it is clear that the minima in transmission spectra are replaced by maxima. The height of the minima together with the known ratio of $\eta_{\text{lum}}/\eta_{\text{scat}}$ gives $q \approx 0.94$ with an uncertainty of at most a factor of 2. The quantum efficiency of unity for $1 \leq v' \leq 6$ of $A\ ^3\Sigma_u^+$ implies that vibrational relaxation causes only a redistribution within the v' levels but no losses to the ground state or to quenching sites by nonradiative processes. The sum over the bars in a histogram of Fig. 5 and Table II has to be 100%.

The samples have been prevented from photons with

TABLE II. Experimental and calculated relative population distribution for N_2 in Xe at 7 K. For details see text.

	Excited v'											
	Experimental						Calculated					
Population	1	2	3	4	5	6	1	2	3	4	5	6
2% N_2/Xe												
N_6						0.09						0.13
N_5					0.16	0					0.15	0
N_4				0.13	0	0.07				0.19	0	0.07
N_3			0.26	0	0.08	0			0.21	0.01	0.07	0.02
N_2		0.26	0	0.12	0.03	0.11		0.42	0	0.14	0.10	0.14
N_1	1.0	0	0.74	0.23	0.67	0.34	1.0	0	0.79	0.60	0.62	0.58
N_0	0	0.74	0	0.52	0.06	0.89	0	0.58	0	0.06	0.06	0.06
0.5 N_2/Xe												
N_6						0.59						0.50
N_5					0.47	0					0.53	0
N_4				0.61	0	0.13				0.60	0	0.15
N_3			0.63	0	0.12	0			0.65	0	0.14	0
N_2		1.0	0	0.12	0.02	0.09		0.75	0	0.11	0.04	0.08
N_1	1.0	0	0.37	0.27	0.29	0.11	1.0	0	0.35	0.26	0.26	0.24
N_0	0	0	0	0	0.10	0.08	0	0.25	0	0.03	0.03	0.03

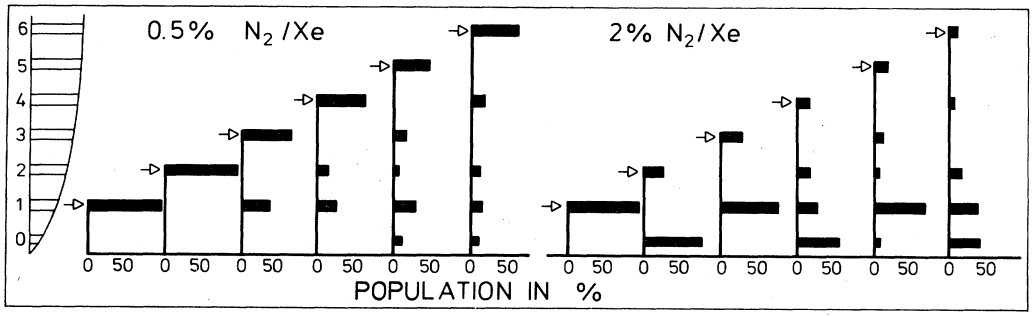

FIG. 5. Experimental population distributions of the vibrational levels of the $A\ ^3\Sigma_u^+$ state for two concentrations of N_2 in Xe. The arrows mark the initially populated state. The length of the bars in a vertical histrogram represents the population.

energies higher than about 9 eV and especially from the background of scattered light and second order in the monochromator output by using a filter. Additional emission bands appear without these precautions, and population distributions similar to those in Fig. 6, are observed. A comparison with Fig. 5 shows that more intermediate levels are populated due to this higher energy background. N_2 molecules are dissociated by higher energy photons and the interaction of N atoms with excited N_2 molecules presumably opens new relaxation channels. This observation is important for a comparison of our results with experiments using high energetic excitation such as electrons or x-rays.

III. DISCUSSION

A. Vibrational relaxation cascade

The discussion will be based on three observations contained in Fig. 5.

(i) Relaxation takes place exclusively in steps of $\Delta v'=2$ for $0\leq v'\leq 3$.

(ii) The initially excited level is depopulated again by $\Delta v'=2$ processes for $4\leq v'\leq 6$ but in the lower part of the cascade also intermediate levels appear which require uneven changes of v'.

(iii) The extent of relaxation increases strongly with N_2 concentration. The majority of the population remains in the initially excited levels for 0.5% N_2 in Xe and it is shifted to lower levels for 2% N_2 in Xe.

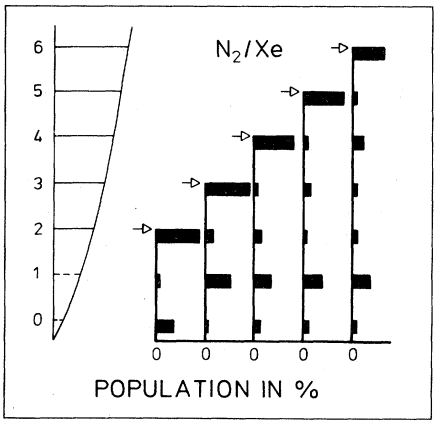

FIG. 6. Population distributions as in Fig. 5 after illuminating a sample with short-wavelength light.

Any simple model of direct dissipation of vibrational energy into matrix phonons would predict only steps of $\Delta v'=1$ because of the energy-gap law.[1,2] The experimental results are incompatible with such a model. The energy-gap law for nonradiative processes postulates a very strong, in general an exponential, decrease of the rate constant with the energy difference between the two energy levels involved or with the number of phonons which have to be emitted. Dissipation of one $A\ ^3\Sigma_u^+$ vibrational quant (174 meV) requires the emission of about 35 matrix phonons with 5 meV energy. Evidently the rate constant for the $\Delta v'=1$ process is too low due to this large number of phonons to compete with radiative decay.

The following model explains observations (i) to (iii) and yields population distributions which agree with the experiment within 10—50 % in nearly all cases. For a discussion of the $\Delta v'=2$ steps we notice that the energy of two $A\ ^3\Sigma_u^+$ vibrational quanta exceeds the energy of one quant of the ground state $X\ ^1\Sigma_g^+$ (292 meV) by only about 50—60 meV [Fig. 7(a), left]. A conversion of two $A\ ^3\Sigma_U^+$ quanta to one ground-state quant, i.e., a $\Delta v'=2$ process should be much more efficient compared with the $\Delta v'=1$ process, because of the much smaller excess energy which corresponds to 10 phonons instead of 35 phonons. The electronic energy of the $A\ ^3\Sigma_u^+$ state has of course to be conserved in this consideration. Therefore a $\Delta v'=2$ process requires the interaction of two N_2 molecules one in the ground state $X\ ^1\Sigma_g^+$ and one in the excited state $A\ ^3\Sigma_u^+$ [Fig. 7(a), right]. The percentage of N_2 molecules which are sufficiently close together for this interaction will increase with N_2 concentration and the degree of relaxation will also increase with concentration. In this way we understand the observations (i) and (iii). The most probable interaction mechanism for relaxation will be a nonresonant nonradiative electronic energy transfer[1,2] from the N_2 molecule (a) to the N_2 molecule (b) [see Fig. 7(a), right]. In a resonant transfer, molecule (a) decays from $A\ ^3\Sigma_u^+(v'+2)$ to $X\ ^1\Sigma_g^+(v''=0)$ and molecule (b) is excited from $X\ ^1\Sigma_g^+(v''=0)$ to $A\ ^3\Sigma_u^+(v'+2)$ without any vibrational relaxation. In the nonresonant case, molecule

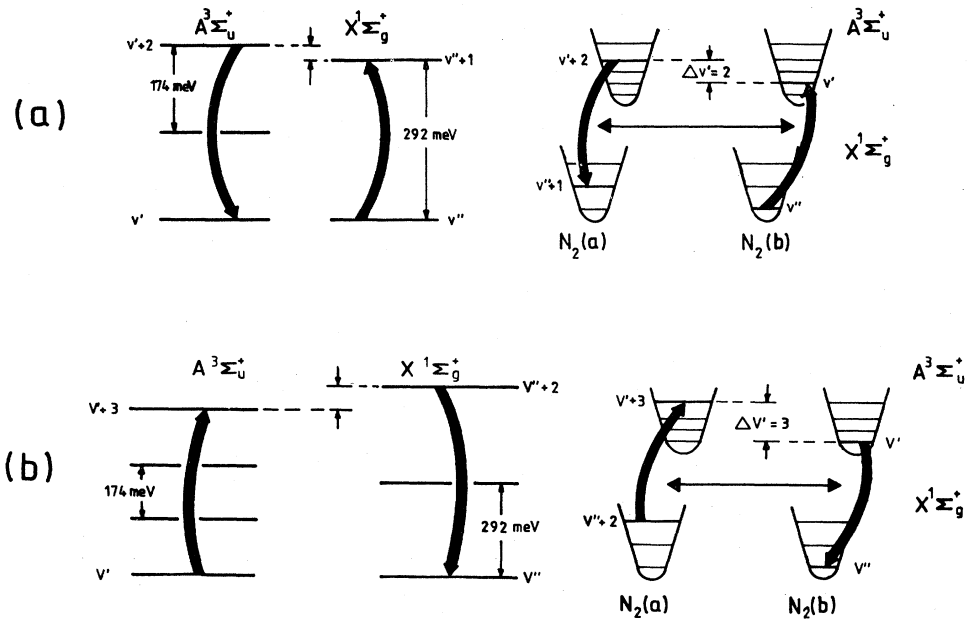

FIG. 7. (a) Illustration of the $\Delta v'=2$ relaxation process in the $A\,^3\Sigma_u^+$ state by nonradiative-energy transfer between the N_2 molecules (a) and (b). (b) Additional $\Delta v'=3$ relaxation channel.

(a) decays from $A\,^3\Sigma_u^+(v'+2)$ to $X\,^1\Sigma_g^+(v''=1)$ and molecule (b) is excited from $X\,^1\Sigma_g^+(v''=0)$ to $A\,^3\Sigma_u^+(v')$. The final result concerning the population of vibrational quanta is a reduction of v' by $\Delta v'=2$ and an increase of v'' by $\Delta v''=1$. The electronic energy jumped from (a) to (b). The excess energy is dissipated to the matrix.

The expected sequences of relaxation processes for different initial levels v' are collected in Fig. 8. The top line for excitation of $v'=1$ shows that no relaxation at all is possible. Initial population of $v'=2$ enables one $\Delta v'=2$ step down to $A\,^3\Sigma_u^+(0)$ and generation of one ground-state vibrational quant $X^1\Sigma_g^+(1)$. A back transfer would add 292 meV of $v''=1$ to $A\,^3\Sigma_u^+(v'=0)$. The resulting excess energy of 120 meV above the next allowed state A

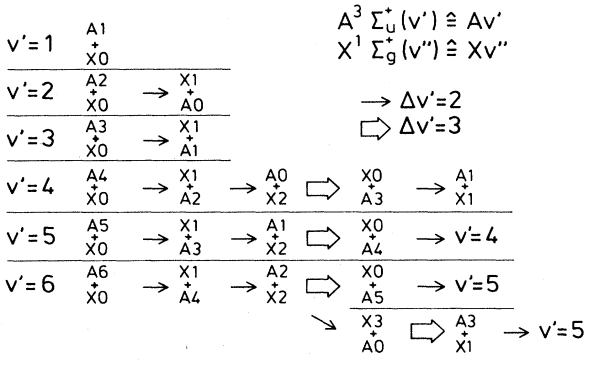

FIG. 8. Scheme for the sequence of energy-transfer steps in relaxation cascades after population of vibrational levels $1<v'<6$ of the $A\,^3\Sigma_u^+$ state. A represents a N_2 molecule in the $A\,^3\Sigma_u^+$ and X one in the $X\,^1\Sigma_g^+$ state. The numbers give the vibrational quanta v' and v''. $\rightarrow$ and $\Rightarrow$ correspond to $\Delta v'=2$ down and $\Delta v'=3$ up conversion processes, respectively.

$^3\Sigma_u^+(v'=1)$ is quite large. This process is less favorable than the $\Delta v'=2$ step and it is not observed in the experimental distributions of Fig. 5. This is an indication that only processes are efficient with energy gaps smaller than 120 meV. Excitation of $v'=3$ leads in one $\Delta v'=2$ step to a similar configuration as the previous $v'=2$ excitation. Only the final $A\,^3\Sigma_u(v'=0)$ state is replaced by $A\,^3\Sigma_u(v'=1)$.

Excitation of $v'=4$ opens a qualitative new channel. Two successive $\Delta v'=2$ steps lead to a configuration of $A\,^3\Sigma_u^+(v'=0)$ at molecule (a) and $X\,^1\Sigma_g^+(v''=2)$ at (b) which is shown in Fig. 7(b). A backtransfer in this case by the decay of $A\,^3\Sigma_u^+(v'=0)$ to $X\,^1\Sigma_g^+(v''=0)$ leads to an excitation of molecule (b) from $X\,^1\Sigma_g^+(v''=2)$ to $A\,^3\Sigma_u^+(v'=3)$. The excess energy in this step is only about 50 meV as is illustrated in the left part of Fig. 7(b). This process is as favorable as the $\Delta v'=2$ step according to the energy-gap law. The backtransfer corresponds to an increase of v' by $\Delta v'=3$ and the uneven change of v' feeds also the intermediate levels. The model predicts population of intermediate levels in the course of relaxation for $v'\geq 4$ in full accord with the experimental finding (ii), and all three observations are reproduced by the model. The $\Delta v'=3$ step is especially interesting because the energy accumulated in one molecule is increased by three v' quanta, i.e., about 500 meV. Vibrational energy stored in the ground state of a molecule can be transferred into an excited electronic state by these nonradiative processes. Vibrational relaxation in this case is not a monotonic flow to lower energies but the energy jumps down and again up in a combination of very specific processes. The up conversion is followed by a step with $\Delta v'=2$ which populates the lower intermediate level $A\,^3\Sigma_u^+(v'=1)$ (see Fig. 8).

A similar series of $\Delta v'=2$ and $\Delta v'=3$ down and up conversion steps is obtained for population of $v'=5$ and

$v'=6$ provided that only processes with an excess energy less than ≈ 100 meV are considered (Fig. 8). For $v'=5$ two steps down with $\Delta v'=2$ lead to $A\ ^3\Sigma_u^+(v'=1)$ and $X\ ^1\Sigma_g^+(v''=2)$. Up conversion by $\Delta v'=3$, raises the energy to $A\ ^3\Sigma_u^+(v'=4)$. The configuration resembles $v'=4$ excitation and the $v'=4$ cascade will proceed. After two $\Delta v'=2$ steps in the $v'=6$ cascade, two pathways with similar energy gaps are possible. Either up conversion to $A\ ^3\Sigma_u^+(v'=5)$ and the whole cascade of $v'=5$ takes place or a further $\Delta v'=2$ step down followed by up conversion and the $v'=5$ cascade starting from the second step.

The rate constants for the nonradiative relaxation and the competing radiative decay are required for a quantitative evaluation of this qualitative picture. In steady state, the sum over all channels I_{ki} which populate level i equals the sum of all depopulating channels $\sum_l I_{il}+\sum_j I_{ij}$ (see Fig. 4). Equation (1) yields, for the population N_i of an intermediate level,

$$N_i=\sum_k w_{ki}N_k \Big/ \left[\sum_l w_{il}+\sum_j w_{ij}\right] , \tag{5}$$

and Eq. (2) gives

$$\sum_l w_{il}=R_e^2\sum_l \nu_{il}^3 \mathcal{F}(i,l) , \tag{6}$$

with $\sum_l \mathcal{F}(i,l)=1$ by definition. We also checked that $\sum_l \nu_{il}^3\mathcal{F}(i,l)$ is independent of i within a few percent when i corresponds to one of the vibrational levels $0\le v'\le 6$ of $A\ ^3\Sigma_u^+$ using the tabulated values of ν_{il} and $\mathcal{F}(i,l)$.[23] This means that there is a common radiative rate constant $w_0=\sum_l w_{il}$ independent on i for those vibrational levels. The experiments of Tinti and Robinson[4] confirm this result for N_2 in Ar and Kr matrices and give a lower bound of $w_0\ge 200\ s^{-1}$ for Xe matrices. In recent experiments, a lifetime of $1.5\times 10^{-3}\pm 0.5$ s (Ref. 15) corresponding to $w_0=600\ s^{-1}$ has been obtained for Xe matrices. Equation (5) can be simplified to

$$N_i=\sum_k \omega_{ki}N_k \Big/ \left[w_0+\sum_j w_{ij}\right] , \tag{7}$$

and the populations can be calculated from the w_0 and the nonradiative relaxation rates ω_{ki} and w_{ij}.

Electronic energy transfer is the driving mechanism in the vibrational relaxation processes. Expressions for multipole interaction where usually the dipole-dipole term dominates and for exchange interaction are well known from the literature.[24] The spin-selection rules reduce the dipole-dipole interaction strongly for the $A\ ^3\Sigma_u^+ - X\ ^1\Sigma_g^+$ states of N_2 and in this case the exchange interaction dominates, as will be discussed in Sec. III B. The rate constant for exchange interaction follows from

$$w_{ex}=\frac{2\pi}{\hbar}\,|\,V_{ab}\,|^2\int f_D(E)F_A(E)dE , \tag{8}$$

with the exchange matrix element V_{ab} and with normalized emission and absorption spectra,

$$\int f_D(E)dE=\int F_A(E)dE=1 . \tag{9}$$

From the manifold of all possible exchange-transfer processes given by w_{ex} we want to extract the rate constant w_{il}^{kj} for the specific channel due to decay of molecule (a) from the ith vibrational level in $A\ ^3\Sigma_u^+$ to the lth level in $X\ ^1\Sigma_g^+$ and for excitation of molecule (b) from the kth vibrational level in $X\ ^1\Sigma_g^+$ to the jth level in the $A\ ^3\Sigma_u^+$. This rate constant is given by the spectral overlap of the two involved transitions in emission and absorption and by still normalizing over all transitions according to Eq. (8). The contribution of the specific decay $i\to l$ to $\int f_D(E)dE$ corresponds to the weighted Franck-Condon factor $\mathcal{F}(i,l)\nu_{il}^3/[\sum_l \nu_{il}^3\mathcal{F}(i,l)]$ and the excitation k-j contributes a value of $\mathcal{F}(k,j)$ to $\int F_A(E)dE$. With these $\mathcal{F}$ factors, the overlap integral is now restricted to the specific transition $i\to l$, $k\to j$ and the line shapes $f_D^{i,l}(E)$ and $F_A^{k,j}(E)$ have to be normalized to

TABLE III. Rate constants w_{il}^{kj} for the decay $A\ ^3\Sigma_u^+(v'=i)\to X\ ^1\Sigma_g^+(v''=1)$ and excitation $A\ ^3\Sigma_u^+(v'=j)\leftarrow X\ ^1\Sigma_g^+(v''=k)$ according to text. ΔE, $A=\mathcal{F}(i,l)\nu_{il}^3\mathcal{F}(k,j)/[\sum_l \nu_{il}^3\mathcal{F}(i,l)]$, and $B=\int f_E^{il}F_A^{kj}dE$ are the energy gaps, Franck-Condon factors, and overlap integrals, respectively, as defined in text.

	ΔE (meV)	A (10^{-3})	B (eV^{-1})	w_{il}^{kj} (s^{-1})
w_{21}^{00}	50	0.16	0.067	1 570
w_{31}^{01}	43	1.25	0.233	42 700
w_{41}^{02}	36	4.2	0.733	451 300
w_{51}^{03}	30	7.8	2.587	2 958 000
w_{61}^{04}	23	9.3	8.396	11 439 000
w_{00}^{23}	46	0.22	0.181	5 800
w_{10}^{24}	57	0.57	0.045	3 800
w_{20}^{25}	67	0.26	0.008	3 000
w_{22}^{10}	61	2.0	0.011	3 200
w_{32}^{11}	54	6.4	0.036	33 000
w_{42}^{12}	47	6.6	0.118	114 000
w_{23}^{20}	61	4.8	0.011	7 700
w_{01}^{33}	35	0.27	1.107	43 800

$$\int f_D^{i,l}(E)dE = \int F_A^{k,j}(E)dE = 1 \ . \tag{10}$$

This yields the energy-transfer rate constants by

$$w_{il}^{kj} = \frac{2\pi}{h} \mid V_{ab} \mid^2 \mathcal{F}(k,j)\mathcal{F}(i,l)v_{il}^3 \left[\sum_l v_{il}^3 \mathcal{F}(i,l) \right]^{-1}$$

$$\times \int f_D^{il}(E) F_A^{kj}(E)dE \ . \tag{11}$$

$\mid V_{ab} \mid^2$ is usually written as

$$\mid V_{ab} \mid^2 = K^2 \exp(-2R/L) \ , \tag{12}$$

with the separation R between molecules (a) and (b), an effective average Bohr radius L and a constant K.[24] The parameters used for the calculation of w_{il}^{kj} and the rate constants are listed in Table III. The Franck-Condon factors[23] and transition frequencies (Table I and Refs. 4 and 23) are available. Fortunately the matrix element V_{ab} has been calculated recently to $\approx 1\ \mathrm{cm}^{-1}$ (1.3×10^{-4} eV) for a pair of two neighboring N_2 molecules in solid N_2.[25] The overlap integral depends on the line shapes and on the energy differences ΔE between the decay and the excitation transitions. The ΔE values of Table III include the Stokes shifts and the anharmonicities in the vibrational progressions. The excitation energies have been derived from our absorption data (Table I). The emission energies follow from the spectroscopic constants given by Tinti and Robinson,[4] which agree with our emission data. The mean value for the Stokes shift of the levels $1 \le v' \le 6$ scattered between 0 and 8 meV for different sets of absorption spectra which indicates the limits of accuracy for the ΔE values.

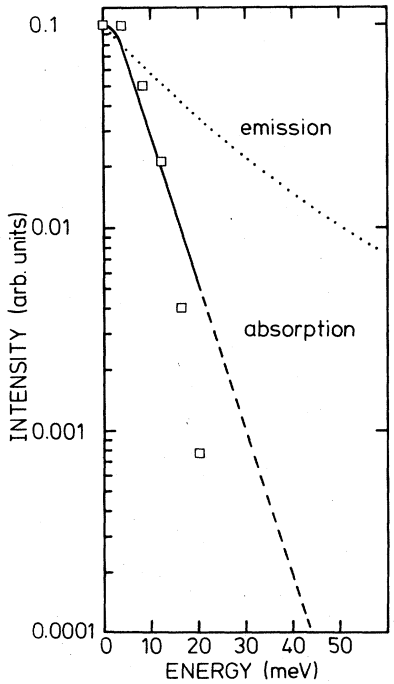

FIG. 9. Comparison of the red wing of the $A\ ^3\Sigma_u^+(v'=1) \rightarrow X\ ^1\Sigma_g^+(v''=9)$ emission band (points) from Ref. 4 with the mirrored blue wing of the $A\ ^3\Sigma_u^+(v'=2) \leftarrow X\ ^1\Sigma_g^+(v''=0)$ absorption band from Fig. 2 (solid line) and with a calculated phonon wing using $S=1$ (squares).

The line shape of the corresponding v' absorption band in Fig. 2 has been used for the excitation part in the overlap integral. The value of the overlap integral is most sensitive to the far red wing of the emission band, because the ΔE values (typically 50 meV) are in general large compared to the full width at half maximum of the emission band (typically 10 meV). The red wing of an emission band[4] shows on a logarithmic scale (Fig. 9) a long tail with decreasing slope. This red wing is caused mainly by inhomogeneous broadening as will be pointed out in Sec. III C. Multiphonon theory in linear coupling predicts, for the emission band, a mirror image of the line shape in absorption. The mirror image of the $X\ ^1\Sigma_u^+(v''=0) \rightarrow A\ ^3\Sigma_u^+(v'=2)$ absorption band decreases faster than the emission bands and shows a constant slope on a logarithmic scale (Fig. 9). It is closer to the homogeneous linewidth which should be caused by electron phonon coupling. A typical line shape predicted by electron-phonon coupling theory is indicated by squares in Fig. 9. The overlap integrals and rate constants have been calculated for the emission band as well as for the mirror image which has been extrapolated by the straight line in Fig. 9. The rate constants derived from the emission bands are one to three orders of magnitude larger than those calculated from the mirror image because of the higher intensity in the red wing around typical ΔE values of 30–60 meV (Table III). The larger rate constants would predict a relaxed population distribution in contradiction to the experiment. The arguments concerning the inhomogeneous broadening, the predictions of electron-phonon coupling theory and the agreement with the experimental population distribution convinced us to use the extrapolated mirror image of the absorption band (Fig. 9) for the line shapes of the decay processes in the overlap integral, yielding the rate constants of Table III.

The concentration dependence of the population distributions (Fig. 5) is due to different distributions of N_2-N_2 separations. For simplification we assume three dominant configurations which are pairs of nearest-neighbor N_2 molecules (N_2-N_2), pairs of N_2 molecules separated by one Xe atom (N_2-Xe-N_2) and completely isolated N_2 molecules. The rate constants for N_2 pairs (N_2-N_2) are given in Table III. The explicit expressions for the populations of the levels in each cascade are collected in Table IV. They are based on Eq. (7) and the selection of rate constants indicated by Fig. 8 and Table III. The evaluation yields the population distribution displayed in Fig. 10. The separation between N_2 molecules in the N_2-Xe-N_2 configuration is about twice that of N_2-N_2 pairs and the exponential distance dependence causes a decrease of the matrix element and thus of all nonradiative rate constants by three to four orders of magnitude.[24] The calculated distributions for the N_2-Xe-N_2 configuration with nonradiative rate constants reduced by a factor of about 2000 are shown in Fig. 10. In isolated N_2 molecules the population in the initial-

TABLE IV. Population N_i of level i according to the cascade displayed in Figs. 4 and 8. w_0 is the radiative rate constant, $w_{ii'}^{kj}$ is the rate constant for nonradiative energy transfer as defined in text and Table III. For excitation of $v'=5$ and 6 the population N_i is given as $N_i=N_i'+N_i''$. The normalization $\sum N_i=1$ has to be added for each level.

	N_i				Population $(N_i=N_i'+N_i'')$ N_i'	N_i''	N_i'	N_i''
N_6							1	0
N_5					1	0	$w_{20}^{25}N_2''/(w_0+w_{51}^{03})$	0
N_4				1	$w_{10}^{24}N_1''/(w_0+w_{41}^{02})$	0	$w_{10}^{24}N_1''/(w_0+w_{41}^{02})$	$w_{61}^{04}/(w_0+w_{42}^{12})$
N_3			1	$w_{00}^{23}N_0/(w_0+w_{31}^{01})$	$w_{00}^{23}N_0'/(w_0+w_{31}^{01})$	$w_{51}^{03}/(w_0+w_{32}^{11})$	$w_{00}^{23}N_0'/(w_0+w_{31}^{01})$	$(w_{01}^{33}N_0''+w_{51}^{03}N_5')/(w_0+w_{32}^{11})$
N_2		1	0	$w_{41}^{02}/(w_0+w_{22}^{10})$	$w_{41}^{02}N_4'/(w_0+w_{22}^{10})$	0	$w_{41}^{02}N_4'/(w_0+w_{22}^{10})$	$w_{42}^{12}N_4''/(w_0+w_{20}^{25}+w_{23}^{20})$
N_1	1	0	w_{31}^{01}/w_0	$w_{31}^{01}N_3/w_0$	$w_{31}^{01}N_3'/w_0$	$w_{32}^{11}N_3''/(w_0+w_{10}^{24})$	$w_{31}^{01}N_3'/w_0$	$w_{32}^{11}N_3''/(w_0+w_{10}^{24})$
N_0	1 0	w_{21}^{00}/w_0	0	$w_{22}^{10}N_2/(w_0+w_{00}^{23})$	$w_{22}^{10}N_2'/(w_0+w_{00}^{23})$	0	$w_{22}^{10}N_2'/(w_0+w_{00}^{23})$	$w_{23}^{20}N_2''/(w_0+w_{01}^{33})$
initial level	0 1	2	3	4	5		6	

ly excited level remains unchanged. Figure 10 illustrates that the population in the lower levels of the relaxation cascades originates from N_2-N_2 pairs, whereas the N_2-Xe-N_2 configurations and isolated N_2 molecules determine the population in the first steps of the cascade and the initial level.

The experimental population distributions are compared with calculated distribution in Fig. 11 and Table II by adding the contributions of 48% isolated N_2, 18% N_2-Xe-N_2 and 48% N_2-N_2 for 0.5% N_2 in Xe and 12% isolated N_2, 8% N_2-Xe-N_2 and 80% N_2-N_2 for 2% N_2 in Xe. We feel that the agreement is quite satisfying in view of the many experimental data from different sources involved in the evaluation. Only the populations of N_0 for exciting $v'=4$ and $v'=6$ in 2% N_2 in Xe are considerably too small. This model explains 54 experimental populations by only using two sets of contributions from isolated N_2, N_2-Xe-N_2, and N_2-N_2 pairs. We want to point out that we use absolute values for the radiative and nonradiative rate constants.

The contributions of different configurations can be compared with expectations based on a statistical distribution of N_2 molecules on substitutional sites of an fcc Xe lattice. Each lattice point in the first three shells around a substitutional N_2 molecule is in the immediate neighborhood of the center N_2 molecule with no further lattice point in between. Therefore N_2 molecules sitting within the first three shells will move to the center N_2 molecule due to the attractive part of the N_2-N_2 potential. The Xe lattice atoms are much larger than the N_2 guests and the guest molecules have space for such a rearrangement.[26] In view of these facts, we consider all N_2 molecules within the first three shells as N_2-N_2 pairs. If a N_2 molecule sits in the fourth shell, then one Xe atom is just in between and the fourth shell is a clear cut N_2-Xe-N_2 case. If a similar rearrangement is to be expected up to the ninth shell is not clear because the attractive force will be much weaker in this case. Since the exchange interaction decreases exponentially we can count either any N_2 molecule beyond the ninth or probably just beyond the fourth shell as isolated. The probability $(1-x)^n$ for a concentration x that no further N_2 molecule is situated within a sphere containing n atoms, yields probabilities for isolated N_2 molecules between $(1-x)^{54}$ and $(1-x)^{248}$, for N_2-N_2 pairs or clusters of $[1-(1-x)^{42}]$ and for N_2-Xe-N_2 between $[(1-x)^{42}$-$(1-x)^{54}]$ and $[(1-x)^{42}$-$(1-x)^{248}]$ (Table V). The values for N_2-N_2 pairs in Table V indicate that the nominal concentrations of 0.5% and 2% correspond to 1% and 4% concerning the number of pairs. An increase of pairs by this amount due to N_2-N_2 interaction seems to be acceptable. For the relative percentages of N_2-Xe-N_2 configurations and isolated N_2 molecules it is not clear how to decide between the extremes of $n=54$ and $n=248$. The experimental values lie in between and are consistent with Table V. A more involved discussion requires an explicit calculation of the rearrangement of the Xe lattice around a substitutional N_2 molecule. In addition nonsubstitutional N_2 sites can be of importance. Inhomogeneous broadening dependent on preparation and complicated concentration dependences in experiments using other excitation sources[15] indicate such site problems.

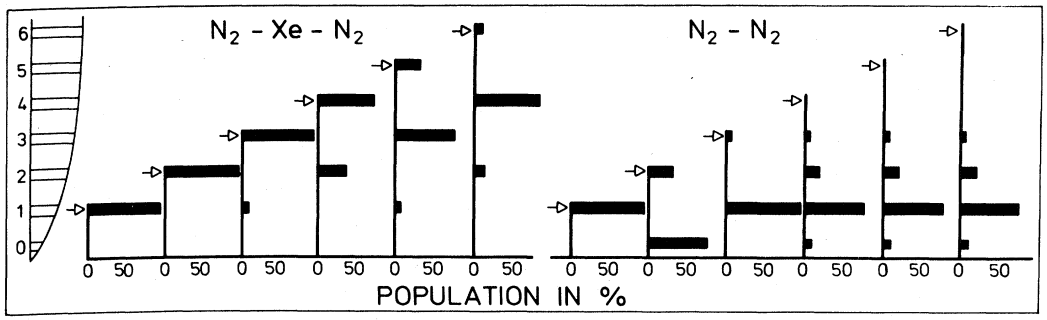

FIG. 10. Calculated population distributions for a N_2-Xe-N_2 configuration and for N_2-N_2 pairs represented as in Fig. 5.

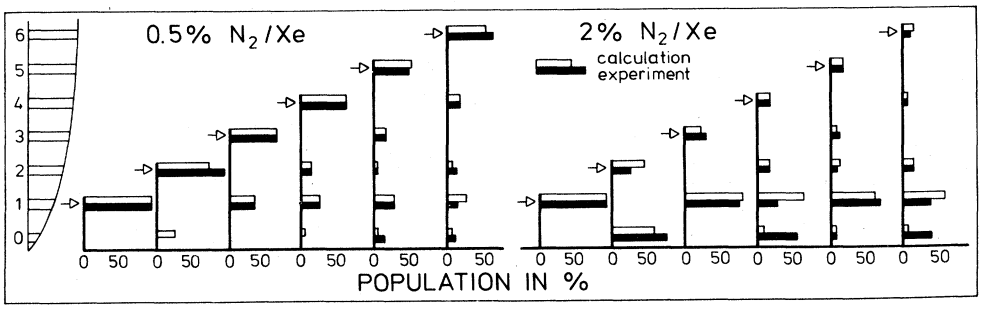

FIG. 11. Experimental and calculated population distributions. The left side represents the experimental results for 0.5% N_2 in Xe compared with a summation for 34% of N_2-N_2 pairs, 18% of N_2-Xe-N_2 configuration and 48% of isolated N_2 molecules. The right side represents the experimental results for 2% N_2 in Xe. Calculation for 80% N_2-N_2 pairs, 8% N_2-Xe-N_2 and 12% isolated N_2.

B. Alternative explanations for the relaxation cascade

In most cases electronic energy-transfer processes are based on dipole-dipole interaction with a rate constant $w_{D\text{-}D}$ given by

$$w_{D\text{-}D}=\frac{3}{2^9\pi^6 cn^6R^6\nu^6\tau^2}\int f_D(E)F_A(E)dE\ , \tag{13}$$

with the velocity of light c, the index of refraction n, the radiative lifetime τ, the transition energy ν in cm^{-1}, and R, f_D, and F_A as before. The ratio of the rate constants for exchange and dipole-dipole interaction, respectively, follows from Eqs. (8) and (13):

$$w_{ex}/w_{D\text{-}D}=|V_{ab}|^2 2^{10}\pi^7 cn^6R^6\nu^6\tau^2/3\hbar\ . \tag{14}$$

The exchange rate constant dominates by a factor of 6×10^6 for a nearest-neighbor N_2 pair and also for a N_2-

TABLE V. Comparison of the statistical probability for N_2-N_2 pairs including larger cluster, for the sum of isolated and N_2-Xe-N_2 configurations, for isolated and for N_2-Xe-N_2 configurations with the results for the nominal experimental concentrations of 0.5% and 2%. For details see text.

		Probability		
Concentration	N_2-N_2	Isolated plus N_2-Xe-N_2	Isolated	N_2-Xe-N_2
Statistical				
0.005	0.19	0.81	0.76—0.28	0.05—0.53
0.010	0.34	0.66	0.58—0.08	0.08—0.56
0.020	0.57	0.43	0.33—<0.01	0.10—0.43
0.030	0.72	0.28	0.19—<0.01	0.09—0.28
0.040	0.82	0.18	0.11—<0.01	0.07—0.18
0.050	0.88	0.12	0.06—<0.01	0.06—0.12
Experimental				
0.005	0.34	0.66	0.48	0.18
0.020	0.80	0.20	0.12	0.08

Xe-N_2 configuration the exchange rate constant is a factor of 2×10^5 larger. Dipole-dipole interaction would be only important for very large separations, but in this case the rate constants are so small that radiative decay has depopulated the excited states.

An alternative explanation of the dominating features in the population distributions by stepwise vibrational relaxation is not possible for the following reasons. Stepwise relaxation predicts necessarily that the population distribution below any initially excited v' level remains unchanged for exciting $v'+1$ or higher vibrational levels which is in clear contradiction to Fig. 5 and Table II. A similar approach would be to involve intersystem crossing from $A\,^3\Sigma_u^+(v')$ to a high-lying nearly resonant level v'' of $X\,^1\Sigma_g^+$ and back relaxation to the next lower level which would be $A\,^3\Sigma_u^+(v'-1)$. This process results in a stepwise relaxation $v'\rightarrow v'-1$ in $A\,^3\Sigma_u^+$ only supported by an intermediate $X\,^1\Sigma_g^+(v')$ level and has to be excluded according to the previous argument. A further way along this line could be intersystem crossing to $X\,^1\Sigma_g^+$, relaxation within the $X\,^1\Sigma_g^+$ vibrational levels thus bypassing some v' levels of $A\,^3\Sigma_u^+$ and back relaxation at one or several distinct $X\,^1\Sigma_g^+$ levels which have a favorable energy resonance with $A\,^3\Sigma_u^+$ levels. Again the distribution within low v' levels of $A\,^3\Sigma_u^+$ should not depend on the initially excited level in contradiction to the experimental result. Furthermore, the severe concentration dependence is not in accord with such intramolecular relaxation processes. The evidently small rate constant for intersystem crossing is not surprising. The electronic matrix element will be small due to the spin-selection rule, the energy-gap law term would be smaller than in the energy-transfer case, because the excess energies which have to be dissipated as phonons are higher and finally the molecular Franck-Condon factor between the involved $A\,^3\Sigma_u^+(0\le v'\le 6)$ and the $X\,^1\Sigma_g^+(25\le v''\le 30)$ levels is only of the order of 10^{-6} and lower. These arguments convinced us that only the proposed energy-transfer processes explains the experimental results in a consistent way.

C. Line shapes, Stokes shifts, and electron-phonon coupling

The homogeneous line shapes of electronic transitions in matrices are caused by electron-phonon coupling and the coupling strength of the transition to the lattice can be for example characterized by the Huang-Rhys coupling constant S.[27] Nonradiative relaxation processes are also induced by the lattice and are described by the same coupling constant. For energy-transfer processes in the Förster-Dexter model this is immediately evident by the appearance of the overlap integral between absorption and emission bands [Eqs. (8) and (13)] and it is true also for more involved descriptions.[1,2,27] For linear coupling, a zero phonon line coinciding in energy for absorption and emission spectra and a mirrorlike progression of phonon side bands extending to the blue in absorption and to the red in emission is expected for temperatures small compared to the phonon energies. In a single-phonon model the phonon side bands are equally spaced by $\hbar\omega_p$ and have intensities $e^{-S}S^N/N!$ with phonon number N.[27] In Fig. 12 the $A\,^3\Sigma_u^+(v'=1)\rightarrow X\,^1\Sigma_g^+(v''=9)$ emission band of

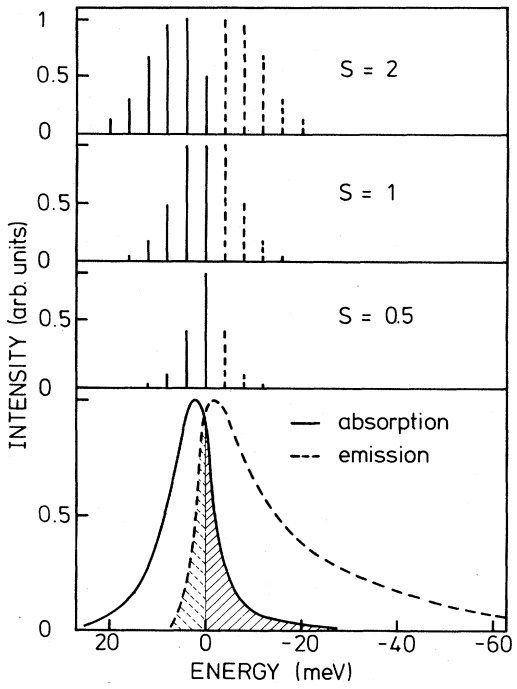

FIG. 12. Line shapes for the $A\,^3\Sigma_u^+(v'=1)\rightarrow X\,^1\Sigma_g^+(v''=9)$ emission band of Ref. 4 (dashed line) and the $A\,^3\Sigma_u^+(v'=2)\leftarrow X\,^1\Sigma_g^+(v''=1)$ absorption bands (solid line) are compared with phonon contours for $S=0.5$, 1, and 2.

Tinti and Robinson[4] is compared with our $A\,^3\Sigma_u^+(v'=2)\leftarrow X\,^1\Sigma_g^+(v=0)$ absorption band after correcting the energies for the different v' and v'' levels involved. This correction causes an uncertainty in the spacing of the maxima from coincidence up to a spacing of 8 meV and a mean value of 4 meV is plotted. Plots of phonon side bands with $\hbar\omega_p=4$ meV and $S=0.5$, 1, and 2 show that the coupling strength is of the order of $S\approx1$. The shadowed overlap of the bands in Fig. 12 cannot be explained by electron-phonon coupling and has to be attributed to inhomogeneous broadening. The correspondence of the red wing in absorption (which is due to inhomogeneous broadening) with the red wing in emission suggests that also the large extension of the red wing in emission is mainly caused by inhomogeneous broadening. The steeper blue wing in absorption is probably closer to the real homogeneous linewidth. This assumption is supported by a comparison of the steepness of the wings with calculated side bands on a logarithmic scale in Fig. 9. The uncertainty in the Stokes shift and the inhomogeneous broadening allow only an estimate of $S\simeq1$ and prevent us to go beyond a single-phonon model or to explain the additional features for higher v' levels in the absorption bands shown in Fig. 2. We mention that an even more complicated behavior of the emissions bands for N_2 in other rare gas matrices has been reported by Creuzburg[15] partly in conflict with our results or the results of Tinti and Robinson.[4]

IV. CONCLUSION

The flow of vibrational and electronic energy in N_2 aggregates in Xe matrices at 7 K has been monitored and a complex interplay of electronic energy transfer and vibrational up and down conversion has been observed. A quantitative description of the hierarchy and the rate constants has been presented. The interpretation in terms of electron-phonon coupling, in connection with the line shape of the optical transitions, is less clear and requires further consideration. The analysis has been concentrated on nonresonant energy-transfer processes leading to a dissipation of molecular vibrational energy into lattice phonons. The rate constants for resonant electronic energy transfer will be of the same order of magnitude. In addition to the processes discussed here transport of electronic energy away from molecules which have been vibrationally excited in the relaxation processes will happen in larger clusters, i.e., at higher concentrations. In a similar way electronic energy can be transported to molecules which are in vibrationally excited states and by up conversion the vibrational population is transferred into the electronically excited state.

We want to point out that the vibrations of N_2 in the electronic ground state represent nonthermal lattice excitations with an energy of 3000 K lasting for seconds in a lattice at 5 K. By the discussed up conversion processes this nonthermal lattice energy can be accumulated in electronically excited molecules thus increasing the total energy in these excited molecules by a considerable amount. Together with the selectivity of the flow of energy demonstrated in this paper new ways for photochemistry in matrices are imaginable.

ACKNOWLEDGMENTS

It is a pleasure to acknowledge fruitful discussions with Dr. Zumofen. In particular he provided us with the matrix element for the exchange interaction and he strengthened the idea of the 3-step-up conversion process. This work has been backed by the crew of the Hamburger Synchrotron Radiation Laboratory (HASYLAB) in Hamburg and has been supported by the Bundesministerium für Forschung und Technologie (BMFT) under Grant Nos. 244 and 245 SW. The lifetime measurement is part of a project in the Sonderforschungsbereich für Struktur und Dynamik von Grenzflächen supported by the Deutsche Forschungsgemeinschaft (DFG).

[1]F. Legay, in *Chemical and Biological Applications of Lasers,* edited by C. B. Moore (Academic, New York, 1977), Part II, p. 43.

[2]V. E. Bondybey and L. E. Brus, in *Advances in Chemical Physics,* edited by I. Prigogine and S. A. Rice (Wiley, New York, 1980), Vol. 41, p. 269.

[3]O. Oehler, D. A. Smith, and K. Dressler, J. Chem. Phys. **66**, 2097 (1977); G. Zumofen, *ibid.* **69**, 4264 (1978); J. Lumin. **18/19**, 887 (1979); Ber. Bunsenges. Phys. Chem. **82**, 128 (1978).

[4]D. S. Tinti and G. W. Robinson, J. Chem. Phys. **49**, 3229 (1968).

[5]H. Y. Sun and S. A. Rice, J. Chem. Phys. **42**, 3826 (1965).

[6]H. J. Jodl and R. Bruno, Phys. Status Solidi B **67**, 191 (1975); **67**, 539 (1975).

[7]I. Ya. Fugol' and Yu. B. Poltoratski, Solid State Commun. **30**, 497 (1979).

[8]M. Creuzburg, Frühjahrstagung der Deutschen Physikalischen Gesellschaft, Würzburg (unpublished).

[9]P. L. Kunsch, Ph.D. thesis, Eidgenössische Technische Hochschule Zürich, 1977.

[10]A. M. Bonnot, Ph. D. thesis, Université D'Aix-Marseille II, 1981.

[11]H. Wilcke, Ph.D. thesis, Universität Kiel, 1983.

[12]J. Sedláček, Ph.D. thesis, Eidgenössische Technische Hochschule Zürick, 1978.

[13]G. Zumofen, J. Sedláček, R. Taubenberger, S. L. Pan, O. Oehler, and K. Dressler, J. Chem. Phys. **81**, 2305 (1984).

[14]F. Coletti and A. M. Bonnot, Chem. Phys. Lett. **45**, 580 (1977).

[15]M. Creuzburg, J. Lumin. **31,/32**, 595 (1984); H. Nahme and N. Schwentner (unpublished).

[16]H. Dubost and R. Charneau, Chem. Phys. **12**, 407 (1976); T. R. Gosnell, R. W. Tkach, and A. J. Sievers, J. Lumin. **31/32**, 166 (1984).

[17]V. E. Bondybey, J. Chem. Phys. **66**, 995 (1977).

[18]J. Goodman and C. E. Brus, J. Chem. Phys. **67**, 4398 (1977).

[19]E. Boursey, V. Chandrasekharan, P. Gürtler, E. E. Koch, P. Kunsch, and V. Saile, Phys. Rev. Lett. **41**, 1516 (1978); P. Gürtler and E. E. Koch, Chem. Phys. **49**, 305 (1980); P. Gürtler, Ph. D. thesis, Universität Hamburg, 1979.

[20]H. Wilcke, W. Böhmer, and N. Schwentner, Nucl. Instrum. Methods **204**, 533 (1983).

[21]P. Gürtler, E. Roick, G. Zimmerer, and M. Pouey, Nucl. Instrum. Methods **208**, 835 (1983).

[22]G. Herzberg in *Spectra of Diatomic Molecules* (Van Nostrand, New York, 1950), p. 200.

[23]A. Lofthus and P. H. Krupenie, J. Phys. Chem. Ref. Data **6**, 113 (1977).

[24]Th. Förster, Z. Naturforsch. **4a**, 321; (1949) D. L. Dexter, J. Chem. Phys. **21**, 836; (1953) M. Inokuti and F. Hirayama, *ibid.* **43**, 1978 (1965).

[25]G. Zumofen (private communication).

[26]G. Theyson, master's thesis, Universität Kaiserslautern, 1977.

[27]D. B. Fitchen, in *Physics of Color Centers,* edited by Fowler (Academic, New York, 1968); J. Jortner, J. Chem. Phys. **64**, 4860 (1976), and in *Vacuum Ultraviolet Radiation Physics,* edited by E. E. Koch, R. Haensel, and C. Kunz (Pergamon, New York, 1974), p. 263; Y. Toyozawa, *ibid.,* p. 317; F. Auzel, in *Luminescence of Inorganic Solids,* edited by Di Bartolo (Plenum, New York, 1978), p. 67.